PNAS RESEARCH ARTICLE | BIOPHYSICS AND COMPUTATIONAL BIOLOGY
APPLIED MATHEMATICS

# Proprioceptive feedback amplification restores effective locomotion in a neuromechanical model of lampreys with spinal injuries

Christina Hamlet[a,1], Lisa Fauci[b], Jennifer R. Morgan[c], and Eric D. Tytell[d]

Edited by Charles Peskin, New York University, New York, NY; received August 3, 2022; accepted January 19, 2023

**Spinal injuries in many vertebrates can result in partial or complete loss of locomotor ability. While mammals often experience permanent loss, some nonmammals, such as lampreys, can regain swimming function, though the exact mechanism is not well understood. One hypothesis is that amplified proprioceptive (body-sensing) feedback can allow an injured lamprey to regain functional swimming even if the descending signal is lost. This study employs a multiscale, integrative, computational model of an anguilliform swimmer fully coupled to a viscous, incompressible fluid and examines the effects of amplified feedback on swimming behavior. This represents a model that analyzes spinal injury recovery by combining a closed-loop neuromechanical model with sensory feedback coupled to a full Navier–Stokes model. Our results show that in some cases, feedback amplification below a spinal lesion is sufficient to partially or entirely restore effective swimming behavior.**

computational fluid dynamics | locomotion | neurophysiology | sensory feedback

## Significance

Lampreys with spinal injuries can often regain functional swimming. After a lesion occurs, the brain cannot activate spinal central pattern generator (CPG) circuits below the lesion. However, if one part of the body can still move, the movement can propagate mechanically across the lesion, which can then be sensed by proprioceptive (body-sensing) neurons. We examine the hypothesis that amplified feedback from these neurons may be sufficient to activate CPG circuits, allowing functional swimming without an activation signal. We show that amplification of certain types of proprioceptive signals below the lesion can restore near-normal swimming behavior. These results shed light on a path to understanding fault tolerance and recovery in vertebrate spinal injuries.

Spinal cord injury in vertebrate animals often causes a partial or complete loss of locomotor abilities. Recovery of locomotion can vary among organisms. While mammals typically experience permanent loss of sensation or movement, many nonmammalian species can partially or completely recover functional locomotion, accompanied by axon regeneration across the lesion site (1–5). For nearly fifty years, lampreys have provided a valuable model organism for studying recovery from spinal injury due to their basal position in vertebrate evolution and the ability to study regenerative processes across scales, ranging from molecular and cellular responses to physiological and behavioral underpinnings (6–13).

Larval lampreys with a spinal injury spontaneously regain swimming behaviors within several weeks after injury (8–11). Functional recovery is supported by regeneration of descending and ascending axons across the injury site, but surprisingly, axon and synapse regeneration is incomplete and sparse. For example, only 30 to 50% of descending axons regenerate across the lesion within the lamprey spinal cord (8–13), and they generate less than 10% of the synaptic connections compared to uninjured axons (9). In addition, there are compensatory changes in the electrophysiological properties of multiple classes of spinal neurons (7, 10). How the spinal central pattern generators (CPGs) overcome the loss of descending commands to restore locomotion is poorly understood, in particular the potential contributions of feedback mechanisms.

One hypothesis is that amplified proprioceptive (body-sensing) feedback can allow an injured lamprey to regain functional swimming, a process that is an example of "fault tolerance" (1), even though the descending signal is lost. Lampreys receive proprioceptive feedback through several intraspinal cell types, the best understood of which are edge cells (15), intraspinal mechanoreceptive cells that sense body curvature and the rate of curvature change (16). Edge cells have a phasic effect, in which they tend to excite activity on the contralateral side and inhibit activity on the ipsilateral side (17), a pattern that tends to terminate activity on the side that is currently active and increases activity on the inactive side. They also have a tonic excitatory effect, in which bending tends to increase the frequency of central pattern generator (CPG) circuits (18, 19). Cells with similar morphology and effects are present in zebrafish (20) and likely in other teleost species. Other cells, including cerebrospinal fluid–contacting cells (21) and dorsal cells (22), may also provide proprioceptive inputs. Indeed, in a robotic model, dorsal cell-like inputs help to stabilize swimming after random damage (23). If such proprioceptors have stronger effects below the lesion after spinal cord injury, it might be possible for the CPG circuits to become active and to synchronize with circuits above the lesion, even without any neural connections. This pattern

Author contributions: C.H., L.F., and E.D.T. designed research; C.H. performed research; C.H., L.F., J.R.M., and E.D.T. analyzed data; and C.H., L.F., J.R.M., and E.D.T. wrote the paper.

The authors declare no competing interest.

This article is a PNAS Direct Submission.



[1]To whom correspondence may be addressed. Email: ch051@bucknell.edu.

This article contains supporting information online at http://www.pnas.org/lookup/suppl/doi:10.1073/pnas.2213302120/-/DCSupplemental.

Published March 10, 2023.

has been observed in leeches, where stretch-receptive neurons can synchronize two segments of the animal, even when the nerve cord is severed (24).

After spinal injury, edge cells become hyperexcitable, and movement-related feedback potentiates the motor output (25, 26). However, there is only a single report of edge cell regeneration (27). Thus, the exact contribution of proprioceptive feedback and how feedback integrates with CPGs to influence behavioral recovery remain largely unknown. Moreover, the role of proprioceptive feedback during normal behavior in uninjured animals is not well understood. For example, when proprioceptive cells are disabled in zebrafish, their movements are much too high amplitude and are poorly coordinated (20).

In this study, we develop numerical simulations of a 2D multiscale, integrative, computational model of a lamprey to investigate the role of local, intraspinal sensory feedback in fault tolerance and functional recovery from spinal cord injury, extending our work examining the role of proprioceptive feedback in locomotion overall (14). Neural signaling is modeled using pairs of coupled phase oscillators along the left and right sides of segments along the lamprey body. These oscillators activate muscles that act on the flexible lamprey body to cause a traveling wave, allowing the lamprey to swim through a fluid that is described by the incompressible Navier–Stokes equations. Fig. 1 shows a schematic of the swimmer's body, its normal CPG, and three different types of neural damage considered here.

While this computational framework can be generalized to other undulatory swimmers, the model presented here is specific to lampreys. First, the tapered body plan and the bending rigidity of the elastic body were chosen to reflect those of lampreys (28, 29). Second, the strength of the neural connections in the phase oscillator model of the CPG driving the motion was based upon experiments on lamprey (30, 31). In addition, we use the work-dependent deactivation muscle model (32, 33) with parameters estimated from lamprey experiments. Finally, the Navier–Stokes equations are solved using the viscosity of water, velocity scales, and spatial scales that reflect the appropriate Reynolds number of lamprey swimming (28).

To close the loop, the emergent curvature of the body acts as an input to the phase oscillator evolution equations (14). Spinal cord injury is modeled by removing connections within the phase oscillator system while keeping the body architecture and tissue properties intact (Fig. 1 *C*–*E*). Our model demonstrates that sensory feedback can compensate for CPG disruption. Sensory feedback can compensate for random failures in a CPG model (23), but it is not known whether changes in feedback gain can help fault tolerance after spinal cord injury. Below we present our model results as a way to explore potential mechanisms for recovery during the initial and acute phases of spinal cord injury, before any neurons have begun to grow across the lesion. We find that amplified feedback below the lesion can be sufficient to permit effective swimming, even with no descending activation of spinal circuits.

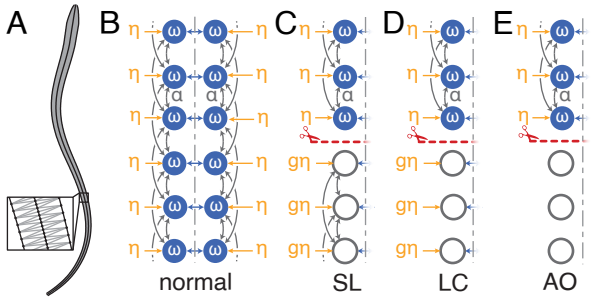


**Fig. 1.** Schematic of the lesion models. (*A*) Schematic of the computational lamprey body, with an inset showing the details of the springs connecting the structural points (full construction given in ref. 14). Panels (*B*–*E*) show the coupled oscillators that drive the activation wave along the body. For all models, filled circles indicate the oscillator's natural frequency $\omega$, and empty circles indicate $\omega = 0$. Gray arrows show the connections among all oscillators on each lateral side with distance-dependent strength $\alpha$. Cross-connections (blue arrows) connect oscillators across a single segment to enforce antiphase relationships on the same segment. The yellow $\eta$ indicates the oscillator feedback, while $g\eta$ indicates amplified feedback. The dotted red line with the scissor icon indicates the lesion, and the vertical gray dash-dot line indicates left–right symmetry. (*B*) "Normal" uninjured CPG. (*C*) "SL type" (spinal lesion). (*D*) "LC type" (loss of connections). (*E*) "AO type " (all off).

## Results

**Cases and Definitions of Feedback Types.** Throughout, the "base case" refers to an uninjured lamprey with no sensory feedback. This is the same base case described in Hamlet et al. (14) (Fig. 1*A*). "Normal" uninjured refers to the case with feedback but with no injury present. The computational model is driven by a set of coupled oscillators described in Eq. **1**. The phase of the oscillator on each side at a particular segment determines the activation state of the muscle at that site. If the sine of the phase is above a prescribed threshold, the oscillator gives an "active" signal, releasing bound calcium that activates muscle contraction on that side of the segment (14).

As in our work (14), to simulate proprioception (15, 17–19), the lamprey receives one of two types of curvature-based feedback during simulations. The first type of feedback signal, labeled "Magnitude-only" (M), is similar to the tonic excitatory effect of edge cell activation (18, 19) and consists of the magnitude of curvature multiplied by a gain, that is, $\eta(\kappa) = g|\kappa|$, where $g$ is the gain multiplier of the signal. The second type of feedback signal, labeled "Directional" (D), is similar to the phasic effect of edge cells (17) and is the curvature magnitude multiplied by gain and assigned as either positive or negative depending on the direction of the curvature measured from head to tail, that is, $\eta(\kappa) = g(sgn(\kappa))|\kappa|$, where $sgn()$ is the sign function and $g$ is the gain multiplier of the signal. The connections associated with each type of injury are summarized in Fig. 1 *C*–*E*.

Three types of injuries at two locations (30% of body length, $L$, and 60% $L$, referred to as high lesion and midbody lesion, respectively) were considered, each with the two different feedback models and different gain multipliers, where appropriate. We compared a control, uninjured case ("normal") to a case that approximates an acute spinal lesion ("SL"). The "normal" case is the uninjured lamprey with all-to-all coupling, with decreasing strength for longer connections, along each side of the body and antiphase coupling across each segment (Fig. 1*B*). The "spinal lesion" injury ("SL": Fig. 1*C*) severs all neural connections between the neurons above the injury and those below the injury. The base frequency of the oscillation ($\omega$) is set to zero below the lesion, representing the loss of descending excitatory input to the CPG, but the local connections are still active. Feedback from local curvature changes is still possible.

We also simulated two additional cases to isolate the roles of feedback and mechanical propagation of a traveling wave. To evaluate the effect of mechanosensory feedback alone, we simulated a case with no connections among oscillators below the lesion, called a "loss of connections" injury ("LC": Fig. 1*D*). Connections among the oscillators will tend to reinforce a traveling wave. The LC case lets us evaluate how well mechanosensory feedback alone can produce a traveling wave. In the LC case, connections are severed across the injury, $\omega = 0$ for oscillators

below the injury, and the coupling between segments is also lost for each oscillator below the cut. Feedback from local curvature change is thus the only mechanism to produce and synchronize a traveling wave below the lesion. Finally, to evaluate the role of mechanics alone, we simulated a completely passive case, in which the region below the injury just deforms based on passive mechanics. In this "all off" case ("AO"; Fig. 1*E*), all connections and feedback from local curvature changes are wholly removed, and $\omega = 0$. This passive case allows us to compare undulatory motions with a passive mechanical traveling wave, which can produce thrust forces e.g., ref. 34, to those motions produced by the CPG-body feedback loop.

Examples of results of the simulations are shown in Fig. 2. Fig. 2*A* shows the wake (vorticity shown in red and blue) produced by the uninjured "base case" (shown in gray) after 8.5 s of simulated time starting from the position shown in red. Fig. 2*B* shows the body waveform of simulations with various types of injuries with magnitude-only feedback after the same amount of simulated time with the same start position. In the absence of feedback (e.g. SLx0, AO), or with little feedback (e.g. SLx1, LCx1), the body waveform and swimming are severely inhibited in the simulated lamprey. However, with increased feedback (e.g. SLx4, SLx10), the simulated lamprey exhibits more normal swimming and body waveforms. Fig. 2 *D*–*F* shows frames from videos of living larval lampreys, illustrating the different stages of injury and recovery and the changes in waveforms compared to the uninjured lamprey (panel *C*). Note how the typical sinusoidal waveform of the swimming lamprey's body returns to normal by 11 wk postinjury.

**With Increased Feedback Gain, Internal Neural Activity below the Lesion Produces a Traveling Wave.** Very little is known about the magnitude of changes in feedback gain after spinal cord injury, although there is some electrophysiological evidence from edge cell recordings that it increases (25). Specifically, a study (25) observed approximately a doubling of firing rate in proprioceptive edge cells, but it is not well understood how this change in firing rate impacts the CPG overall. Here, we chose to bracket a range of possible changes, to understand whether changes in feedback gain might have a potential to affect functional recovery. Fig. 3 shows the activation pattern in swimmers with a midbody lesion and different types of feedback. Fig. 3*A* shows left and right side activation (dark and light gray, respectively) relative to time and body position, where a diagonal band represents a steady traveling wave. With magnitude-only feedback and a gain of 4×, the swimmer begins to produce a traveling wave below the lesion (Fig. 3*A*3). Fig. 3*B* shows representative activity on the right side for three segments along the body. Fig. 3*C* shows the synchronization between oscillators across the lesion and within the segment below the lesion, where a value of 1.0 indicates that oscillators are exactly synchronized and 0.0 indicates complete lack of synchrony. With a gain of 10×, the swimmer has robust phase locking across the lesion, similar to the base case (compare Fig. 3, column 4 to column 1, both outlined in bold), despite lacking any neural connections across the lesion. Similarly, the 10× gain case has a clear traveling wave, as shown by the diagonal bands in Fig. 3*A*. With directional feedback (columns 5 and 6), a fast oscillation and a slow oscillation occur. Increasing the multiplier below the injury in these cases increases the frequency and amplitude of the rapid oscillation. Still, it can produce some synchronization across the lesion (Fig. 3*C*6). These oscillations represent a quick reversal of the activation signal, resulting in the noisy signal seen in Fig. 3 *A*5 and *A*6.

**Higher Gain Produces Traveling Waves of Bending, Leading to Higher Swimming Speed.** Fig. 4*A* shows the emergent swimming kinematics due to the interaction of neural activation, muscle force, and external fluid forces. With a high lesion (at 30%), many of the swimmers develop a standing wave pattern, but with sufficiently high magnitude-only feedback, a traveling wave of bending develops (e.g., Fig. 4*A*, SL×10, leading to a higher swimming speed (Fig. 4*B*1). With a midbody lesion (at 60%L; bottom two rows), the swimmer develops a traveling bending wave above the lesion, which then propagates across the lesion, where it can be reinforced by sensory feedback. Fig. 4*B* shows the time evolution of swimming speeds for the two different feedback types (in columns) and the two lesion locations (top row, 30%; bottom row, 60%). The swimmers that develop traveling wave

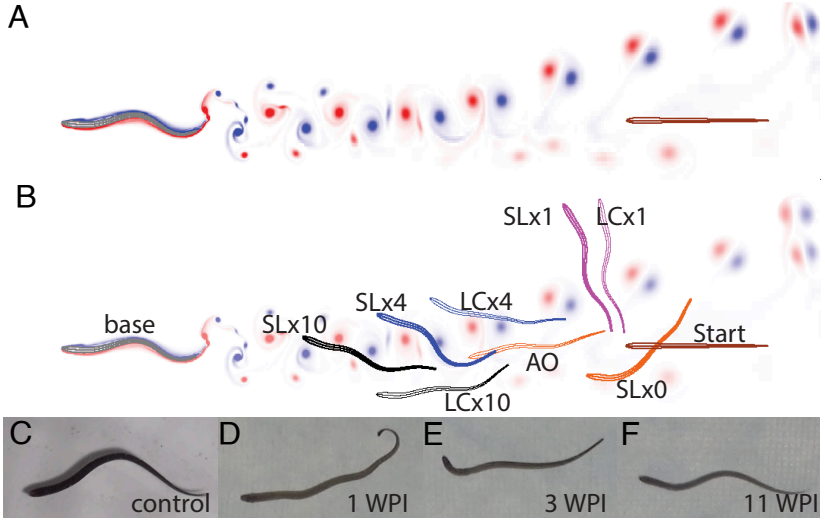


**Fig. 2.** Waveforms of injured computational and living lampreys. (*A*) Wake of a computational lamprey simulation with no injury, where red and blue represent counterclockwise and clockwise vorticity, respectively. The dark red body outline shows the starting point of the simulation. (*B*) Computational lampreys shown at the same point in simulated time with injury at 30% body length (*L*), magnitude-only feedback, and "SL," "AO," and "LC" type connections as labeled. The gray swimmer is the base case (no feedback, no injury). Each of the remaining colors has a different multiplier amplifying feedback below the injury: orange = 0× (no feedback below tail), pink = 1× (normal feedback), blue = 4×, and black=10×. "Start" shows the starting point of each of the simulations. Images of swimming larval lampreys (*C*) before injury, (*D*) 1 wk postinjury (WPI), (*E*) 3 WPI, and (*F*) 11 WPI. Images provided by Dr. Hilary Katz, Western Kentucky University.

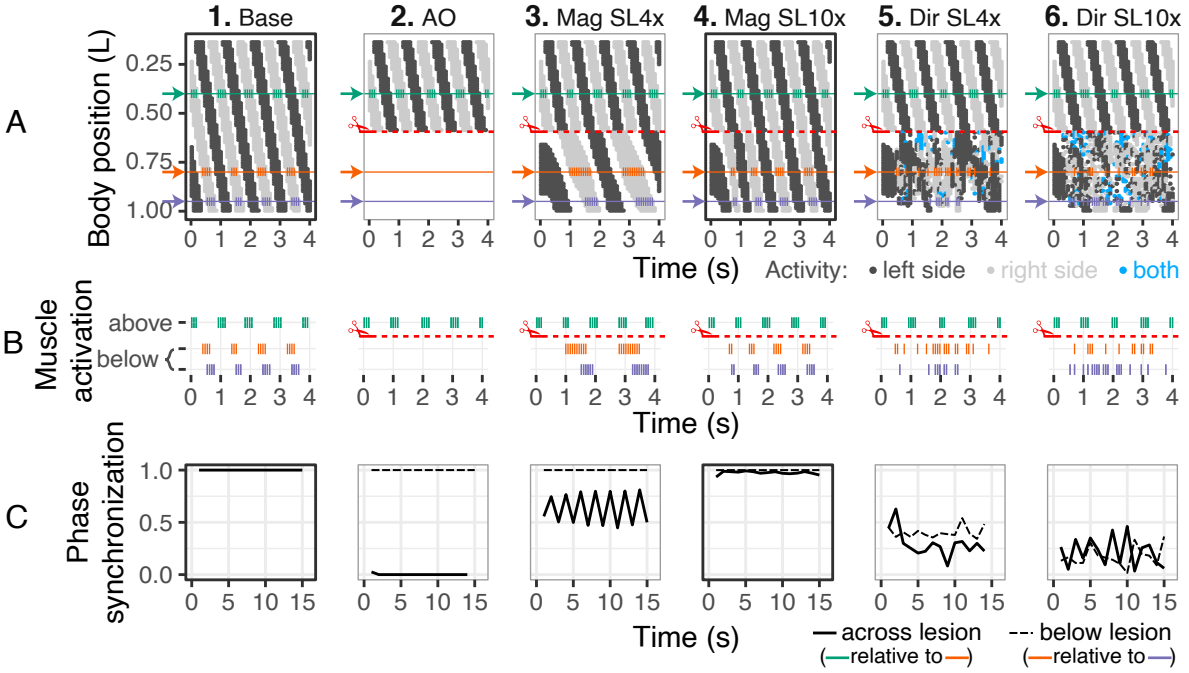


**Fig. 3.** Traveling waves and synchronized activity can be produced with sufficiently high feedback gain. Panels show results from the base case and the AO and SL type injuries with a lesion at 60%*L* (red dashed line). Columns represent different feedback models: 1, Base; 2, AO; 3, SL magnitude-only $g = 4$ below the injury; 4, SL magnitude-only $g = 10$ below the injury; 5, SL directional $g = 4$ below the injury; 6, SL directional $g = 10$ below the injury. (*A*) Activation signals along the body, where dark gray and light gray represent left and right side activation, respectively. Representative activity from panel *B* is shown superimposed. (*B*) Activation signals on the right side, above the lesion, and at two positions below the lesion for the first 4 s of simulated time. (*C*) Rayleigh's *R* metric of synchronization, which indicates stable phase offsets between oscillators across the lesion (solid line) and between the two positions below the lesion (dashed line), where 1.0 represents perfect synchronization and 0 indicates completely unsynchronized signals. *Methods* for details. The panels outlined in bold indicate the recovery of a stable traveling wave (column 4) close to the base case (column 1).

patterns (e.g., SL×10) reach the highest speeds, and for lesions at 60%, they reach speeds similar to the base case (Fig. 4 *B*3 and *B*4).

**Injuries Reduce Performance in All Swimmers.** Even though many of the swimmers do achieve some forward swimming speed, the loss of connections across the spinal lesion always resulted in a less efficient swimmer. This loss of performance can be seen qualitatively in Fig. 4*B*, where each swimmer's center of mass speed is lower than the base case (*SI Appendix*, Movies S1–S6). Following (32, 35), we estimated the metabolic cost of transport by assuming that muscle requires energy proportional to the magnitude of mechanical work performed but that negative mechanical work requires less energy than positive work. Injured swimmers generally required 2 to 4 times more energy than uninjured swimmers, although at high feedback gain (8× or 10×), the cost of transport was only slightly higher than the base case (*SI Appendix*, Fig. S1).

## Discussion

This is an integrative neuromechanical model that simulates the coupling between body, muscle, and fluid mechanics together with proprioceptive mechanosensory feedback, as a way to examine functional changes in spinal cord injury. This model builds on our previous work (14), in which we examined the effect of different classes of curvature feedback on swimming performance in a simulated lamprey-like swimmer. Here, we "injured" the model and showed that in all conditions tested, proprioceptive feedback enhanced swimming performance. Remarkably, with sufficiently strong excitatory sensory feedback (our "magnitude-only" class, similar to that observed experimentally by Kiemel (19)), swimmers can regain near-normal swimming with midbody lesions (Fig. 4*B*3) and effective, though slower than normal, swimming with a high lesion (Fig. 4*B*1). These data suggest that feedback amplification could contribute to functional recovery.

**Recovery of Swimming with Amplified Feedback.** Based on evidence that proprioceptors may become hypersensitized after spinal cord injury (25), we explored the effect of computationally increasing feedback gain below the lesion. In a variety of animal species, proprioceptive sensory inputs are crucial to recovery from spinal cord or nerve cord injury. The leech *Hirudo verbana* is able to recover locomotor behavior after its nerve cord is severed, because proprioceptors, which normally contact only one ganglion, grow and synapse in multiple ganglia (36)—a potential form of the amplification we tested here. Cats with spinal cord injury can recover some stepping ability after spinal cord injury (37), but only if proprioceptors remain intact (38).

In our model, swimmers with magnitude-only feedback could achieve near-normal swimming speeds at gains of 8× or 10×, even for the high lesions (Fig. 4 *B*1 and *B*2). These swimmers develop a fairly normal traveling activation wave (Fig. 3*A*4). This effect seems largely to be driven by feedback, and not by intersegmental coupling, because the LC swimmers also swam effectively, although they did swim slightly slower than their SL counterparts (*SI Appendix*, Fig. S2). These results together indicate that sufficient amplification of proprioceptive signals can compensate for the loss of connections in certain types of spinal injuries.

**The Mechanical Wave Appears to Support and Stabilize the Activation Wave with Sufficient Feedback Amplification.** In the cases of the midbody injuries (60%*L*), as feedback below

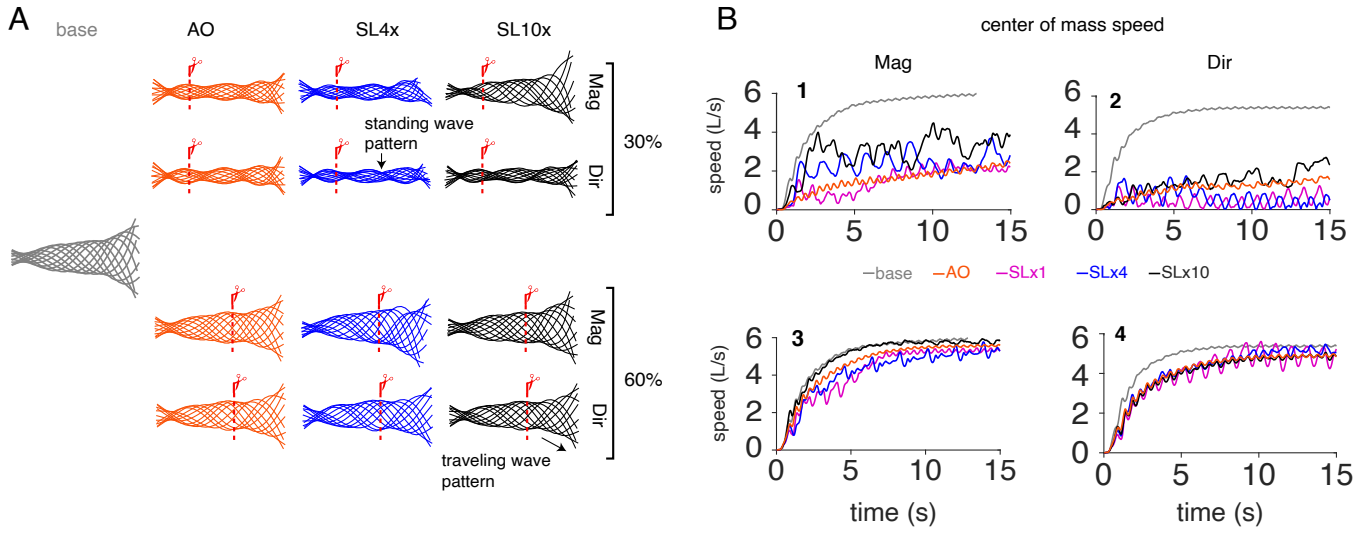


**Fig. 4.** Midline movements and swimming speed for different feedback types and gains. (*A*) Midline traces of the base case, and AO- and SL-type injured lampreys over a full tailbeat cycle. The red dashed line indicates the site of the injury. The head of the lamprey is on the left of each plot. (*B*) Center of mass speed for each of the midline cases shown in the corresponding row to the left. The first row shows data from lesions at 30% and the second row at 60%. Columns represent different feedback types.

the injury is amplified, the activation wave approaches a pattern closer to the CPG of an uninjured lamprey (Fig. 3*A*4). Even though connections are severed across the injured region, a mechanical wave builds up above the injury and propagates mechanically toward the tail (Fig. 4*A*). Proprioceptors below the lesion then can activate and synchronize activity to that mechanical wave (Fig. 3*C*4), at least for magnitude-only feedback. The directional feedback does cause more fluctuation of the activity but at high-enough amplification levels can begin to synchronize with the mechanical wave (Fig. 3*C*6) to stabilize the overall swimming pattern and produce a traveling wave (Fig. 4 *A*, *Bottom* row). Even in the purely passive case (AO), the injured animal can swim relatively effectively, as has been seen in other studies of passively flexible tails or panels (29, 34, 39).

In the high lesions (30%*L*), there is less of an uninjured region to initiate a mechanical traveling wave. Most cases develop a standing wave pattern (Fig. 4, *Top* rows), and only with the highest feedback do we see a traveling wave developing. The connections along the spinal cord (Fig. 1, gray lines) reinforce the traveling wave, which likely explains why the SL case, which has these connections, swims faster than the LC case, which lacks the connections (compare speeds in Fig. 4*B* to *SI Appendix*, Fig. S2).

Thus, a propagating mechanical wave can stabilize the neural signal in some situations. These results with directional feedback further indicate that even in cases where feedback is insufficient to reestablish a stable neural signal, it can still contribute to stabilization from the mechanical wave. For leeches, a propagating mechanical wave can serve to synchronize segments across a nerve cord lesion (24).

**Neuromechanical Processes for Fault Tolerance.** Our results suggest that animals can potentially recover locomotor performance, even in the face of complete spinal cord injury, by tuning in to the fundamental mechanics of their bodies (1). A mechanical wave can propagate passively along an injured section of a body lacking neuromuscular activity. This mechanical coupling can synchronize two sections of the body that are disconnected neurally, provided that proprioceptive feedback is sufficiently strong. Our model did not simulate any regeneration across the lesion, which is a crucial aspect of recovery in lampreys (1–5, 8–13). However, regenerated axons make fewer and shorter connections across the lesion than in intact animals (9), and thus, we hypothesize that lampreys may benefit from the increased edge cell sensitivity or synaptic weights below the lesion, as has been demonstrated or suggested in prior studies (25, 26, 40). Although a prior study suggested minimal influence of mechanosensory feedback in the dissected lamprey spinal cord preparation (40), this was not formally tested. Nor were the contributions of local feedback from intraspinal neurons assessed in the dynamically locomoting preparation, as was modeled here. Furthermore, in vertebrates ranging from lampreys to humans, the compensatory neural plasticity that occurs within spinal locomotor networks in response to injury appears to be complex and includes both circuit reorganization as well as alterations in intrinsic and synaptic properties of both sensory and motor neurons (25, 26, 41, 42). Neuromodulation achieved by electrical stimulation or pharmacological approaches may additionally boost sensory feedback to improve functional recovery after spinal injury (43–45). In our model, a 10× gain was required to achieve normal activity, but this was achieved in the absence of any regeneration across the lesion or alterations in the CPG network. Both of these processes—regeneration and circuit-level plasticity—occur during recovery from spinal cord injury in lampreys (10–13), which suggests that functional recovery in the living animal may not require such a large amplification of proprioceptive feedback. Despite the potential for restoring locomotor functions, enhancing neural activity and modulatory gain may also contribute to spasticity or neuropathic pain associated with spinal cord injury (46, 47). Our computational findings prompt the need for a deeper understanding of the feedback mechanisms that contribute to postinjury recovery and, in particular, how enhanced feedback integrates with spinal CPGs at the circuit level, and we argue that this should be a focus area in future studies (1). Moreover, there is a growing need to understand how enhanced feedback after injury could help restore function while also keeping spasticity and pain in check.

Humans and other legged animals also tune into the mechanical properties of their limbs to enhance locomotion; for example, matching the mechanical resonant frequency of leg swing

(48). Robots can synchronize decoupled limbs by mechanical interactions, given appropriate mechanosensory feedback (49). Thus, a potential therapeutic approach for spinal cord injury may be to search for ways to increase the sensitivity or activity of proprioceptors below the lesion.

## Materials and Methods

We use an immersed boundary framework (e.g., refs. 50–52) that models the lamprey body (of length $L = 12.6$ cm) as a neutrally buoyant, elastic actuated structure immersed in a viscous, incompressible fluid. In order to resolve the flow at the appropriate Reynolds number, we use an adaptive method where the underlying finite difference grid adapts dynamically to add resolution in spatial regions coinciding with immersed boundary points of the lamprey structure as well as regions of high vorticity (53). The computational domain is a rectangle of dimensions 7.5L by 6L, with no-slip boundary conditions on top and bottom and no penetration on the sides. Further details are provided in refs. 28 and 14.

**Model Construction and Parameters.** The computational lamprey consists of three segmented filaments, a stiff centerline and two lateral sides, shown in Fig. 1*A* (*Inset*). The links along the center filament and the crosslinks that connect the centerline to the lateral sides are modeled as passive, Hookean springs. The links along the lateral sides are modeled as springs, but they do not resist compression. These links divide the lateral sides into 320 segments that also support active muscle contractions. The swimmer is constructed using 1,284 points, 321 points along each lateral side, and 642 points down the body's centerline. Forces are generated along the body by inserting a Hill-type muscle model between neighboring points on the lateral sides. A system of ordinary differential equations describing calcium dynamics governs the contraction of each muscle segment. The calcium equations are, in turn, driven by a neural activation signal modeled using a system of weakly coupled oscillators. The details of the activation wave are given below, along with the construction of sensory feedback models. The activation wave generated by the oscillators drives muscle contractions along the lateral sides using a kinetic model described in refs. 28, 32 and 14 and based on a model from ref. 33.

**Activation Wave Equations.** The central pattern generator is modeled as two chains of coupled oscillators. There are 320 segments: the first 40 are passive (meant to represent the "head"), and the remaining 280 are connected to oscillators. Each segment has two oscillators governed by

$$\dot{\theta}_{k,i} = \omega_{k,i} + \sum_{j=1}^{n} \alpha_{ij} \sin(\theta_{k,j} - \theta_{k,i} - \psi_{ij}) + a_c \sin(\theta_{k,i} - \theta_{k*,i} + \pi) + \eta(\kappa_{k,i}) \quad [1]$$

where $\theta_{k,i}$ is the $2\pi$-periodic *ith* oscillator on the *kth* side of the body in the chain, $\omega$ is the uncoupled angular frequency of the oscillators, $\alpha_{ij}$ is the coupling strength between segments $i$ and $j$, $a_c$ is the cross-coupling of oscillators on the same segment, and $\psi_{ij}$ is the preferred phase lag between oscillators. Following ref. 54, the preferred phase lag is about 1% per segment in the natural lamprey. Our integrative model has three times as many segments for numerical purposes, so we set a phase lag of $\psi_{ij} = 0.0035 * 2\pi * (i - j)$. The parameter $\eta(\kappa_{k,i})$ is the feedback term that depends on the value of the curvature at segment $i$. $k$ indicates the "left" 1) or "right" 2) lateral side of the lamprey.

To construct the proprioceptive model for the oscillators on both the right and left sides of the body, a smoothed value of the curvature at the corresponding centerline segment is used. This curvature evolves from the coupled fluid/body mechanics of the system.

In Fig. 3*C*, synchronization between two oscillators was assessed using Rayleigh's $R = \sqrt{S_{i-j}^2 + C_{i-j}^2}$ where $S_{i-j} = \frac{1}{N}\sum_p \sin\left[\theta_i(t_p) - \theta_j(t_p)\right]$ and $C_{i-j} = \frac{1}{N}\sum_p \cos\left[\theta_i(t_p) - \theta_j(t_p)\right]$ (55). We computed phase locking in each half oscillation cycle, by computing the oscillation frequency $T$ in the region above the lesion, then looking at windows of time with duration $T/2$.

**Data, Materials, and Software Availability.** CSV and text for documentation, data have been deposited in LabArchives. The data are stored and publicly available at: https://dx.doi.org/10.25833/dj9y-pk02.

**ACKNOWLEDGMENTS.** We thank Dr. Hilary Katz of Western Kentucky University for footage of injured lampreys (Fig. 2 *C–F*) taken at the Marine Biological Laboratory. This work was supported by NSF IOS 1652582 to E.D.T., by NSF CBET 916154 to C.L.H., NSF DMS 1951707 for L.J.F., and by the Marine Biological Laboratory Eugene Bell Center Endowment, Rowe Endowment for Regenerative Biology, and Charles Evans Research Development funds to J.R.M.

Author affiliations: [a]Department of Mathematics, Bucknell University, Lewisburg, PA 17837; [b]Department of Mathematics, Tulane University, New Orleans, LA 70118; [c]The Eugene Bell Center for Regenerative Biology, Marine Biological Laboratory (MBL), Woods Hole, MA 02543; and [d]Department of Biology, Tufts University, Medford, MA 02155

1. G. Haspel *et al.*, Resilience of neural networks for locomotion. *J. Physiol.* **599**, 3825–3840 (2021).
2. J. Morgan, M. Shifman, *Non-Mammalian Models of Nerve Regeneration*, M. Selzer, S. Clarke, L. Cohen, G. Kwakkel, R. Miller, Eds. (Cambridge University Press, ed. 2, 2014), vol. **1**, pp. 329–338.
3. J. P. Rasmussen, A. Sagasti, Learning to swim, again: Axon regeneration in fish. *J. Exp. Neurol.* **287**, 318–330 (2016).
4. S. Rossignol, A. Frigon, Recovery of locomotion after spinal cord injury: Some facts and mechanisms. *Ann. Rev. Neurosci.* **34**, 413–440 (2011).
5. E. M. Tanaka, P. Ferretti, Considering the evolution of regeneration in the central nervous system. *Nat. Rev. Neurosci.* **10**, 713–723 (2009).
6. A. H. Cohen, S. A. Mackler, M. E. Selzer, Functional regeneration following spinal transection demonstrated in the isolated spinal cord of the larval sea lamprey. *Proc. Natl. Acad. Sci. U.S.A.* **83**, 2763–2766 (1986).
7. R. M. Cooke, D. Parker, Locomotor recovery after spinal cord lesions in the lamprey is associated with functional and ultrastructural changes below lesion sites. *J. Neurotrauma* **26**, 597–612, PMID: 19271969 (2009).
8. K. L. Hanslik *et al.*, Regenerative capacity in the lamprey spinal cord is not altered after a repeated transection. *PLoS One* **14**, 1–27 (2019).
9. P. A. Oliphint *et al.*, Regenerated synapses in lamprey spinal cord are sparse and small even after functional recovery from injury. *J. Comp. Neurol.* **518**, 2854–2872 (2010).
10. D. Parker, The lesioned spinal cord is a "new" spinal cord: Evidence from functional changes after spinal injury in lamprey. *Front. Neural Circuits* **11** (2017).
11. C. M. Rovainen, Regeneration of müller and mauthner axons after spinal transection in larval lampreys. *J. Comp. Neurol.* **168**, 545–554 (1976).
12. M. E. Selzer, Mechanisms of functional recovery and regeneration after spinal cord transection in larval sea lamprey. *J. Physiol.* **277**, 395–408 (1978).
13. A. D. McClellan, Brainstem command systems for locomotion in the lamprey: Localization of descending pathways in the spinal cord. *Brain Res.* **457**, 338–349 (1988).
14. C. L. Hamlet, K. A. Hoffman, E. D. Tytell, L. J. Fauci, The role of curvature feedback in the energetics and dynamics of lamprey swimming: A closed-loop model. *PLoS Comput. Biol.* **14**, 1–29 (2018).
15. S. Grillner, T. L. Williams, P. Å. Lagerbäck, The edge cell, a possible intraspinal mechanoreceptor. *Science* **223**, 500–503 (1984).
16. N. Massarelli, A. Yau, K. A. Hoffman, E. D. Tytell, T. Kiemel, The encoding properties of mechanosensory edge cells in the lamprey spinal cord. *J. Comp. Physiol. A Neuroethol. Sens. Neural Behav. Physiol.* **203**, 831–841 (2015).
17. G. Viana Di Prisco, P. Wallén, S. Grillner, Synaptic effects of intraspinal stretch receptor neurons mediating movement-related feedback during locomotion. *Brain Res.* **530**, 161–166 (1990).
18. L. Guan, T. Kiemel, A. H. Cohen, Impact of movement and movement-related feedback on the lamprey central pattern generator for locomotion. *J. Exp. Biol.* **204**, 2361–2370 (2001).
19. T. Kiemel, A. H. Cohen, Bending the lamprey spinal cord causes a slowly-decaying increase in the frequency of fictive swimming. *Brain Res.* **900**, 57–64 (2001).
20. L. D. Picton *et al.*, A spinal organ of proprioception for integrated motor action feedback. *Neuron* **109**, 1188–1201e7 (2021).
21. U. L. Böhm *et al.*, CSF-contacting neurons regulate locomotion by relaying mechanical stimuli to spinal circuits. *Nat. Commun.* **7**, 1–8 (2016).
22. J. Christenson, A. Boman, P. Å. Lagerbäck, S. Grillner, The dorsal cell, one class of primary sensory neuron in the lamprey spinal cord. I. Touch, pressure but no nociception – a physiological study. *Brain Res.* **440**, 1–8 (1988).
23. R. Thandiackal *et al.*, Emergence of robust self-organized undulatory swimming based on local hydrodynamic force sensing. *Sci. Rob.* **6**, eabf6354 (2021).
24. X. T. Yu, W. O. Friesen, Entrainment of leech swimming activity by the ventral stretch receptor. *J. Comp. Physiol. A: Neuroethol. Sensory Neural Behav. Physiol.* **190**, 939–949 (2004).
25. N. Hoffman, D. Parker, Interactive and individual effects of sensory potentiation and region-specific changes in excitability after spinal cord injury. *Neuroscience* **199**, 563–576 (2011).
26. M. Becker, D. Parker, Time course of functional changes in locomotor and sensory systems after spinal cord lesions in lamprey. *J. Neurophysiol.* **121**, 2323–2335, PMID: 31017839 (2019).
27. H. Yin, M. Selzer, Axonal regeneration in lamprey spinal cord. *J. Neurosci.* **3**, 1135–1144 (1983).
28. E. D. Tytell, C. Y. Hsu, T. L. Williams, A. H. Cohen, L. J. Fauci, Interactions between internal forces, body stiffness, and fluid environment in a neuromechanical model of lamprey swimming. *Proc. Natl. Acad. Sci. U.S.A.* **107**, 19832–19837 (2010).
29. E. D. Tytell *et al.*, Role of body stiffness in undulatory swimming: Insights from robotic and computational models. *Phys. Rev. Fluids* **1**, 073202 (2016).

30. A. H. Cohen *et al*., Modeling of intersegmental coordination in the lamprey central pattern generator for locomotion. *Trends Neurosci.* **15**, 434–438 (1992).
31. P. Várkonyi, T. Kiemel, K. Hoffman, A. Cohen, P. Holmes, On the derivation and tuning of phase oscillator models for lamprey central pattern generators. *J. Comp. Neuro.* **25**, 245–261 (2008).
32. C. Hamlet, L. Fauci, E. Tytell, The effect of intrinsic muscular nonlinearities on the energetics of locomotion in a computational model of an anguilliform swimmer. *J. Theor. Biol.* **385** (2015).
33. T. Williams, A new model for force generation by skeletal muscle, incorporating work-dependent deactivation. *J. Exp. Biol.* **213**, 643–50 (2010).
34. P. Leroy-Calatayud, M. Pezzulla, A. Keiser, K. Mulleners, P. M. Reis, Tapered foils favor traveling-wave kinematics to enhance the performance of flapping propulsion. *Phys. Rev. Fluids* **7**, 074403 (2022).
35. A. Ruina, J. E. Bertram, M. Srinivasan, A collisional model of the energetic cost of support work qualitatively explains leg sequencing in walking and galloping, pseudo-elastic leg behavior in running and the walk-to-run transition. *J. Theor. Biol.* **237**, 170–192 (2005).
36. J. G. Puhl, A. W. Bigelow, M. C. P. Rue, K. A. Mesce, Functional recovery of a locomotor network after injury: Plasticity beyond the central nervous system. *eNeuro* **5** (2018).
37. S. Rossignol *et al*., Locomotor capacities after complete and partial lesions of the spinal cord. *Acta Neurobiol. Exp. (Wars)* **56**, 449–463 (1996).
38. L. Carrier, E. Brustein, S. Rossignol, Locomotion of the hindlimbs after neurectomy of ankle flexors in intact and spinal cats: Model for the study of locomotor plasticity. *J. Neurophysiol.* **77**, 1979–1993 (1997).
39. D. B. Quinn, G. V. Lauder, A. J. Smits, Scaling the propulsive performance of heaving flexible panels. *J. Fluid Mech.* **738**, 250–267 (2014).
40. A. D. McClellan, Time course of locomotor recovery and functional regeneration in spinal cord-transected lamprey: In vitro preparations. *J. Neurophysiol.* **72**, 847–860, PMID: 7983540 (1994).
41. D. Parker, The functional properties of synapses made by regenerated axons across spinal cord lesion sites in lamprey. *Neural Regen. Res.* **17**, 2272–2277 (2022).
42. A. C. Smith, M. Knikou, A review on locomotor training after spinal cord injury: Reorganization of spinal neuronal circuits and recovery of motor function. *Neural. Plast* **2016**, 1216258 (2016).
43. E. Svensson, O. Kim, D. Parker, Altered GABA and somatostatin modulation of proprioceptive feedback after spinal cord injury in lamprey. *Neuroscience* **235**, 109–118 (2013).
44. S. Harkema, C. Angeli, Y. Gerasimenko, Historical development and contemporary use of neuromodulation in human spinal cord injury. *Curr. Opin. Neurol.* **35**, 536–543 (2022).
45. B. R. Noga, J. D. Guest, Combined neuromodulatory approaches in the central nervous system for treatment of spinal cord injury. *Curr. Opin. Neurol.* **34**, 804–811 (2021).
46. N. B. Finnerup, Neuropathic pain and spasticity: Intricate consequences of spinal cord injury. *Spinal Cord* **55**, 1046–1050 (2017).
47. Q. Yang *et al*., Persistent pain after spinal cord injury is maintained by primary afferent activity. *J. Neurosci.* **34**, 10765–10769 (2014).
48. B. K. Ahlborn, R. W. Blake, W. M. Megill, Frequency tuning in animal locomotion. *Zoology (Jena)* **109**, 43–53 (2006).
49. D. Owaki, T. Kano, K. Nagasawa, A. Tero, A. Ishiguro, Simple robot suggests physical interlimb communication is essential for quadruped walking. *J. R. Soc. Interface* **10**, 20120669 (2013).
50. A. P. Hoover, R. Cortez, E. D. Tytell, L. J. Fauci, Swimming performance, resonance and shape evolution in heaving flexible panels. *J. Fluid Mech.* **847**, 386–416 (2018).
51. M. Santiago, N. A. Battista, L. A. Miller, S. Khatri, Passive concentration dynamics incorporated into the library IB2d, a two-dimensional implementation of the immersed boundary method. *Bioinspiration Biomimetics* **17** (2022).
52. O. Maxian, A. T. Kassen, W. Strychalski, A continuous energy-based immersed boundary method for elastic shells. *J. Comput. Phys.* **371**, 333–362 (2018).
53. B. E. Griffith, R. D. Hornung, D. M. McQueen, C. S. Peskin, An adaptive, formally second order accurate version of the immersed boundary method. *J. Comput. Phys.* **223**, 10–49 (2007).
54. J. Previte, N. Sheils, K. Hoffman, T. Kiemel, E. Tytell, Entrainment ranges of forced phase oscillators. *J. Math. Bio.* **62**, 589–603 (2011).
55. N. I. Fisher, *Statistical Analysis of Circular Data* (Cambridge University Press, Cambridge, 1995).